

Article

# Biodiesel Production by Esterification Reaction on K<sup>+</sup> Modified MgAl-Hydrotalcites Catalysts

Chen-Yang Zhang <sup>1,2</sup>, Wen-Li Shao <sup>1</sup>, Wei-Xia Zhou <sup>1</sup>, Yang Liu <sup>1,2</sup>, Yuan-Yuan Han <sup>1,2</sup>, Yi Zheng <sup>1</sup> and Yong-Jun Liu <sup>1,2,\*</sup>

<sup>1</sup> College of Chemical Engineering, Huaqiao University, Xiamen 361021, China

<sup>2</sup> Institution of Chemical Process and Intrinsic Safety, Huaqiao University, Xiamen 361021, China

\* Correspondence: yongjunliu@hqu.edu.cn; Tel.: +86-592-6162300

Received: 4 August 2019; Accepted: 27 August 2019; Published: 2 September 2019



**Abstract:** K<sup>+</sup> modified hydrotalcites and its activity as a solid base catalyst for ultrasonic wave-assisted biodiesel conversion was investigated. The solid alkaline catalysts of the MgAl-hydrotalcites (HT) was prepared by co-precipitation and modified with K<sup>+</sup> by impregnation. The influence of K<sup>+</sup> incorporation on the performance of Mg-Al hydrotalcites catalysts was investigated by SmartLab X-ray powder diffractometer (XRD), infrared spectrum (IR), thermogravimetric-differential thermal analysis (TG-DTA), CO<sub>2</sub> temperature programmed desorption (CO<sub>2</sub>-TPD), scanning electron microscopy (SEM), and N<sub>2</sub> adsorption-desorption isotherm (BET). The research discovered that K<sup>+</sup> modified of double layered structure of MgAl-hydrotalcite resulted in a significant increase in catalytic activity in transesterification of rapeseed oil. It exhibited high catalytic activity that achieved a biodiesel yield of 99% when the reaction was conducted with 2 wt% catalysts, K<sup>+</sup>/HT load ratio of 6.25%, a methanol/rapeseed oil molar ratio of 12:1, and reaction at 60 °C over 1 h. The result showed that the K<sup>+</sup> modified HT as a transesterification catalyst had the potency for biodiesel conversion. In addition, under the above reaction conditions, the biodiesel yield was up to 99.9% in only five minutes with ultrasonic aid.

**Keywords:** MgAl hydrotalcites; solid alkaline; biodiesel; K<sup>+</sup> modified; ultrasonic aid

## 1. Introduction

Biodiesel refers to a nonpetroleum-based fuel that can be used in compression-ignition engines, produced from renewable biological resources such as triglycerides (plant oils and animal fats), generally composed of fatty acid methyl esters (FAME) or fatty acid ethyl esters (FAEE) [1–4]. It was prepared by transesterification of triglyceride with lower alcohol under catalyst conditions. Various catalysts, such as homogeneous acids, homogeneous bases, heterogeneous acids, heterogeneous bases, and biological enzymes, have been reported for biodiesel production [5–8]. The transesterification rate of the homogeneous base is more than the homogeneous acid, which is about 4000 times that of the latter, and thus more widely used [9]. Conventional biodiesel was mostly prepared by homogeneous alkali catalytic process, which has some disadvantages such as heavy pollution, difficult recycling of catalyst, and easy deactivation of catalyst by water and free fatty acids in raw materials [10]. In recent years, solid base catalysts have been attracting extensive attention due to their high catalytic activity and reusability [11]. This type of catalyst is used in biodiesel synthesis and includes supported catalysts such as KI/Al<sub>2</sub>O<sub>3</sub> [12], K<sub>2</sub>CO<sub>3</sub>/Al<sub>2</sub>O<sub>3</sub>-SiO<sub>2</sub> [13], and metal oxides such as CaO [14], ion-exchange resin [15], and Hydrotalcite-like anionic clay [16].

Hydrotalcite with layered double hydroxides is a new type of layered material with a special structure and function [17]. The general formula of hydrotalcites can be written as  $[M_{1-X}^{2+}M_X^{3+}(\text{OH})_2]^{X+}(\text{A}^{n-})_{X/n}\cdot m\text{H}_2\text{O}$ , where the divalent metal cations M<sup>2+</sup> are replaced by a trivalent

metal cation  $M^{3+}$  to change the layer structure and enhance the alkali strength of the catalyst [18]. However, the as-prepared hydrotalcites are often inactive in base-catalyzed reaction because their pores contain a large amount of water with physical adsorption which hinders the access to basic sites [19]. Calcined hydrotalcite materials have few active sites. Therefore, the solid base catalysts of hydrotalcite modified by alkali metal salts, such as  $K^+$  or  $Na^+$ , are favored by many researchers in biodiesel synthesis. Hájek et al. used the calcined MgFe-layered double hydroxides (LDHs) to catalyze rapeseed oil with methanol, and the maximum yield of biodiesel was only 70% [20]. Benedictto et al. studied the  $Na^+$  or  $K^+$  doped MgAl-HT which were able to catalyze sunflower oil, and found that the potassium-containing materials had a better catalytic effect with 80% yield of biodiesel [21]. These catalysts have characteristics such as adjustable structure, structure memory function, easy separation from reaction products, and simple after-treatment, but also possess the problems of high preparation difficulty and weak alkalinity.

In this work,  $K_2CO_3/MgAl-HT(K^+/HT)$  catalyzed rapeseed oil with methanol to synthesize biodiesel. The incorporation of  $K^+$  made it exhibit high alkalinity, high catalytic activity, and high stability. At the same time, the strengthening effect of ultrasound aid on transesterification was also discussed. Furthermore, the results showed that the reaction rate can be greatly improved by ultrasonic aid. The purpose of this research was to obtain the biodiesel with economically and environmentally friendly methods.

## 2. Results and Discussion

### 2.1. Catalysts Characterization

The XRD patterns of  $K^+/HT$  catalysts with different  $K^+$  loading are shown in Figure 1. They exhibited that all of samples had the characteristic peaks of calcined HT composite oxide  $Mg(Al)O$  at  $2\theta = 41.5^\circ, 62.0^\circ$ . The phenomenon indicated that all the samples retained the LDHs structure, which is the characteristic structure of hydrotalcites. When the  $K^+$  loading was 2.50 wt%, the formation of strong alkaline active species was not obvious, and no typical characteristic peak appeared. Of note was that the signals began to appear with 3.75 wt% loading, which were attributed to the results of reaction between  $K^+$  and HT. The signals of the  $K_2O$ , Al-O-K, and Mg-O-K phases can be clearly observed and enhanced with increasing of  $K^+$  loading [22–25]. The increasing of these active species was obviously beneficial to the enhancement of the alkali activity of the  $K^+/HT$  catalyst, which was favorable for the transesterification reaction. However, excessive loading may cause adverse effects, such as surface coverage and pore blockage.

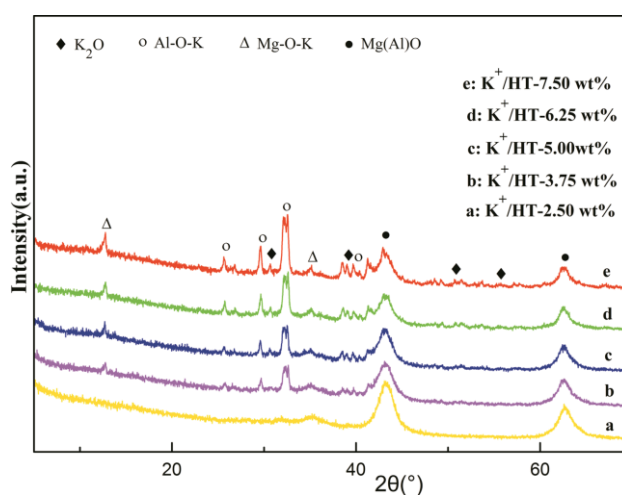


Figure 1. XRD patterns of  $K^+/HT$  with different  $K^+$  loadings.

The fourier transform infrared spectra of the  $K^+/HT$ -6.25 wt% samples before and after calcination were shown in Figure 2. Bands at  $3430\text{ cm}^{-1}$  of uncalcined catalyst can be attributed to the  $-OH$  stretching vibration in the layered structures, and the ones of calcined samples were assigned to the Al-O-K stretching vibration [26]. Vibrations located at  $1373\text{ cm}^{-1}$ ,  $784\text{ cm}^{-1}$ , and  $665\text{ cm}^{-1}$ , associated with interlayered carbonates ( $CO_3^{2-}$ ), clearly appeared in the uncalcined sample. However, vibrations in the corresponding location did not appear in the calcined catalyst because of decomposition of  $CO_3^{2-}$  in the catalyst after calcination. The bands at  $1430\text{ cm}^{-1}$  and  $858\text{ cm}^{-1}$  of calcined catalyst can be attributed to the K-O stretching vibration from  $K_2O$  and  $K^+$  incorporated Mg(Al)O composite oxide completely [27]. The bands corresponding to the stretching vibration of Mg-O phase in the calcined product were presented at  $456\text{ cm}^{-1}$ , which was mutually confirmed by the aforementioned XRD results.

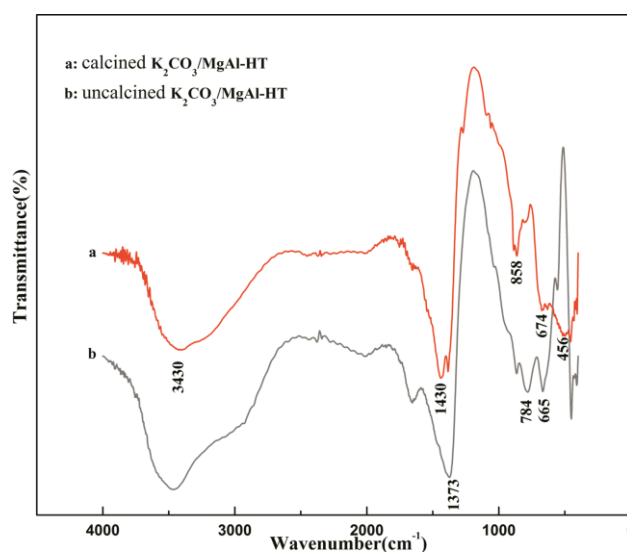


Figure 2. Infrared spectra of the calcined and uncalcined  $K^+/HT$ .

The TG-DTA curves of the uncalcined  $K^+/HT$ -6.25 wt% sample are presented in Figure 3. The research demonstrated that there were three major weight-loss processes when the sample was calcined from  $25\text{ }^\circ\text{C}$  to  $1000\text{ }^\circ\text{C}$ . The first weight-loss step in TG occurred below  $250\text{ }^\circ\text{C}$  and the amount was about 11.7%, which was mainly the removal of adsorbed water and crystal water of hydrotalcite interlayer. The second weight-loss was shown in the range of  $250\sim 600\text{ }^\circ\text{C}$  and the mass loss was approximately 24%, which corresponded to the dehydroxylation of the OH groups in Mg-Al brucite-like sheets and decomposition of the interlayer  $CO_3^{2-}$  anions [28]. The biggest weight-loss was presented at around  $335\text{ }^\circ\text{C}$ , and the layer structure was destroyed during this stage. The third weight-loss was observed at the temperature range  $600\sim 1000\text{ }^\circ\text{C}$ . Additionally, two endothermic peaks appeared successively, which were assigned to the thermal effects of the change of the crystal phase (the formation of Al-O-K, Mg-O-K) and the removal of the remaining hydroxyl in the HT framework. When the temperature exceeded  $850\text{ }^\circ\text{C}$ , the catalysts began to sinter and form a spinel phase. From the above analysis, the calcination at a higher temperature was beneficial to the formation of highly active species, but the catalyst will turn into an inert spinel structure at high temperatures [29,30].

The BET surface, pore size, and average pore volume of  $K^+/HT$ , MgAl-HT, and MgAl-HT (calcination of  $700\text{ }^\circ\text{C}$ ) were characterized and listed in Table 1. As shown in Table 1, the specific surface area and pore volume of the catalysts increased after calcination and loading. The higher surface area of the calcined samples can be associated with the release of interlayer water molecules and carbon dioxide from carbonate anions. Figure 4 demonstrates that the BET isotherm of the  $K^+/HT$  catalysts was type IV and had an H3 hysteresis loop. After calcination, the hydrotalcite layer structure collapsed and

the pore type was the slit hole produced by particle stacking. The pore size distribution demonstrated that the pore size of the catalyst was narrow, and the average pore diameter was 3.834 nm.

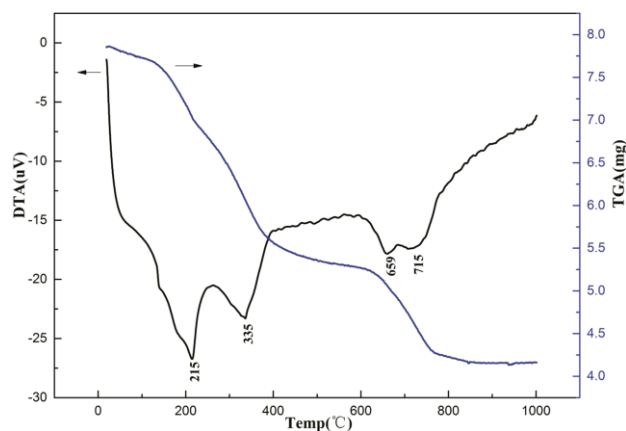


Figure 3. TG-DTA curves of the uncalcined  $K^+$ /HT sample.

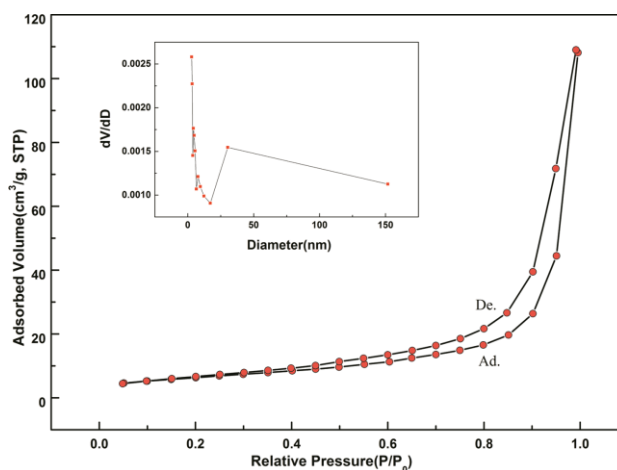


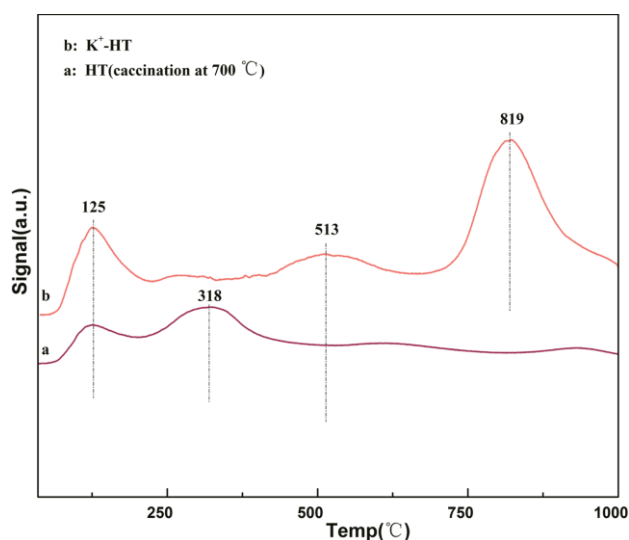
Figure 4. Nitrogen adsorption–desorption isotherms and pore size distribution curve of  $K^+$ /HT.

Table 1. Pore structure properties of the catalysts.

Sample	BET Surface Area ( $m^2 g^{-1}$ )	Pore Volume ( $cm^3 g^{-1}$ )	Pore Size (nm)
$K_2CO_3/MgAl-HT$	109.286	0.421	3.825
MgAl-HT (calcination at 700 °C)	123.885	0.513	3.834
MgAl-HT	91.153	0.323	3.822

For solid basic catalysts, the amount of irreversibly adsorbed  $CO_2$  reflects the population of base sites on exposed surfaces. The desorption temperature indicates the adhesion strength of adsorbate on the base site. The results for temperature-programmed desorption of  $K^+$ /HT-6.25 wt% and the calcined MgAl-HT product are presented in Figure 5. A significant low temperature desorption peak (125 °C) and a medium temperature desorption peak (318 °C) on the Mg(Al)O desorption curve of calcined HT product indicated that only the weak base and medium strong base locations are provided by the surface hydroxyl and Mg(Al)O ion pairs. Two high temperature desorption peaks (513 °C and 819 °C) were observed on the desorption curve of  $K^+$ /HT, in addition to the low temperature desorption peak (125 °C), and the total area of desorption peaks was also higher than that of Mg(Al)O, which implied that the introduction of  $K^+$  increased the alkali strength and the number of basic sites of

the catalyst. The two high temperature desorption peaks corresponded to the formation of strong basic sites of active species  $K_2O$  and  $M-O-K$  ( $M = Mg, Al$ ), and the weakening of the medium temperature desorption peak was also caused by  $K^+$  entering the lattice of  $Mg(Al)O$ .



**Figure 5.**  $CO_2$ -TPD curves of  $K^+/HT$  and calcined  $MgAl-HT$ .

The SEM micrographs were shown in Figure 6, corresponding to the hydrotalcite-like materials ( $K^+/HT$ ). The  $K^+/HT$  catalysts showed a fluffy multi-porous structure and exhibited a typical blade-like morphology. This morphological structure was obviously beneficial to expose more active sites and facilitate the diffusion of larger molecules of oil reactants. The results showed that the reactants were more likely to enter the reactive center to increase the efficiency in the transesterification reaction.

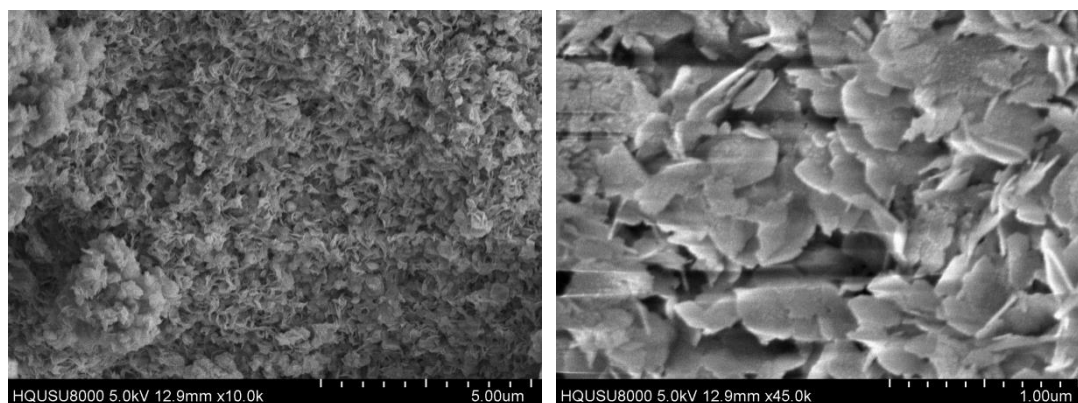


**Figure 6.** SEM images of the  $K^+/HT$  with different resolutions.

## 2.2. Catalytic Performance for Biodiesel Production

A series of transesterification reactions were performed by using the solid alkaline catalyst of  $K^+$  modified hydrotalcite, and the optimized reaction conditions were investigated by varying the different parameters. The effect of ultrasound aid on transesterification was also studied under optimized reaction conditions.

### 2.2.1. Effect of $K^+$ Loading Ratio

Figure 7a demonstrates the influence of the different loading amounts of  $K^+$ . Under the same conditions, the biodiesel yield was increased with the increasing of  $K^+$  loading. Figure 7a exhibits that the transesterification activity of the catalysts reached the maximum when the  $K^+$  loading was

6.25 wt%, and then the activity decreased as the  $K^+$  loading increased. The explanation was that excessive  $K^+$  loading tends to agglomerate the active species on the surface of a limited catalyst and block the catalyst pores, which caused the decrease of catalyst activity.

#### 2.2.2. Effect of Methanol/Oil Molar Ratio

As is well-known, the stoichiometric ratio for transesterification is 3:1 (methanol/oil). However, an excess of methanol will increase the oil conversion by shifting this equilibrium to producing methyl ester. In Figure 7b, the ester yield increased as the molar ratio increased, and reached a maximum of 99% with a molar ratio of 12:1. As the molar ratio continued to increase, the yield decreased slightly, which was attributed to a large amount of methanol diluting the oil and decreasing the reaction rate.

#### 2.2.3. Effect of the Amount of Added Catalyst

Figure 7c demonstrates that when the amount of the catalyst was 2 wt%, the yield reached a maximum, and the yield of the biodiesel decreased as the amount of the catalyst increased. This phenomenon was explained as follows: the catalyst had provided sufficient surface and active center in the reaction system until the amount of catalyst reached the supersaturation state, and the rate controlling step of the transesterification reaction was changed from the original methanol adsorption control to the mass transfer control. A large amount of glycerin, one of the products of transesterification reaction, covered the surface of the catalyst and diluted the methanol concentration near the reaction center. Furthermore, the excess alkaline center easily caused side reactions, such as saponification and hydrolysis.

#### 2.2.4. Effect of the Reaction Temperature

Figure 7d shows that the yield increased with the increase of temperature in the range of 40 to 60 °C. The maximum of yield was up to 99% at 60 °C. Then the yield decreased with the increase of temperature. The main reason is that the equilibrium constant was obviously affected by the reaction. Therefore, as the temperature increased, the conversion rate of the oil rose. In addition, when the reaction temperature was close to 64.7 °C (the boiling point of methanol), the system was strongly turbulent, which was beneficial to strengthen mass transfer and increase the reaction rate. However, as the temperature continued to increase, a large amount of methanol bubbles appeared on the surface of the catalyst, due to the large amount of methanol vaporization, hindering the mutual contact of the reactants and the catalyst, and thereby lowering the reaction rate and decreasing the biodiesel yield.

#### 2.2.5. Effect of the Reaction Time

The effect of reaction time on biodiesel yield is shown in Figure 7e. The results exhibited that the biodiesel yield reached 85% when the reaction was carried out for fifteen minutes. However, as the reaction time was increased to one hour, the yield was as high as 99%. The FAME yield was ideal with the reaction time of one hour, from Figure 7e.

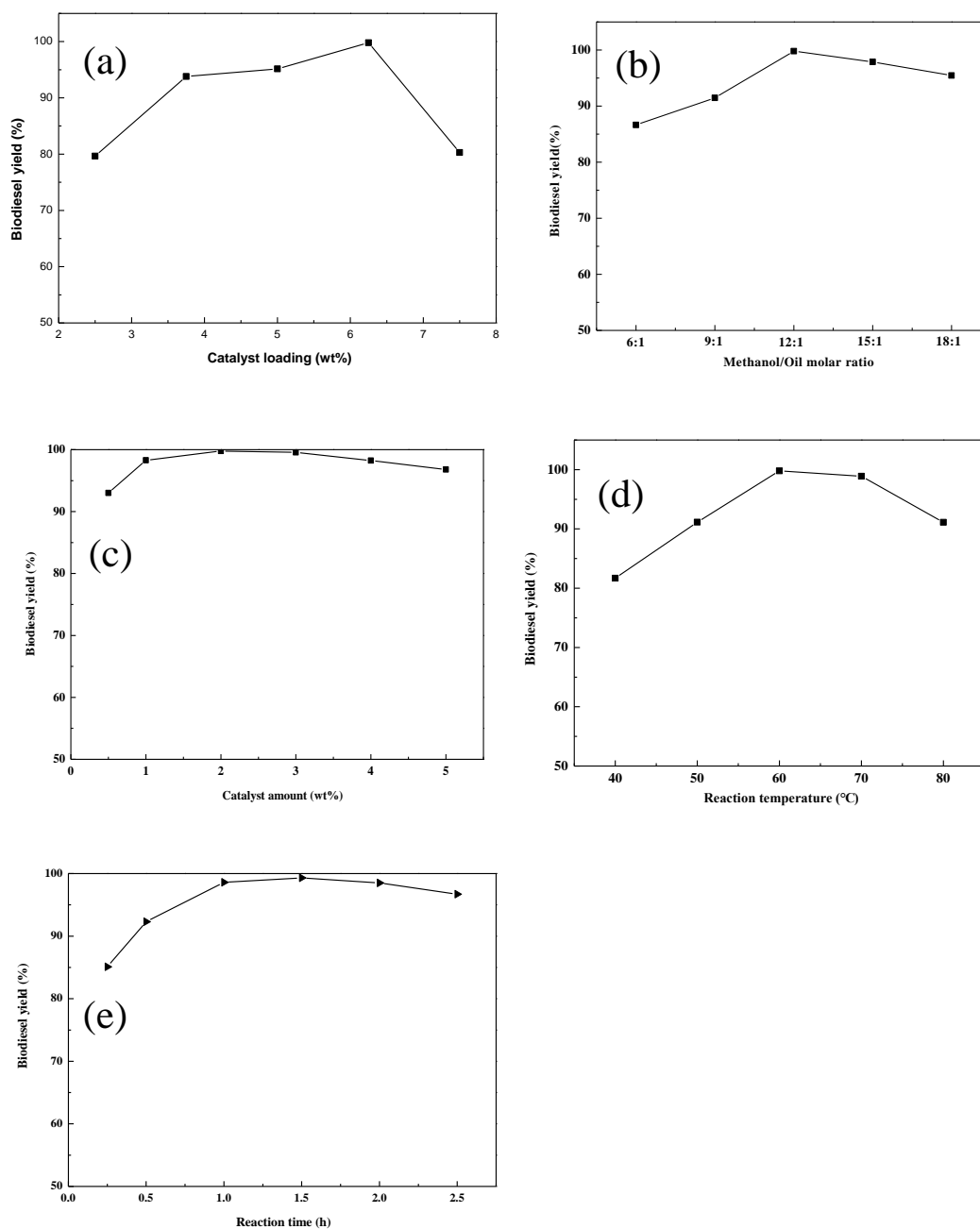


**Figure 7.** Effects of the reaction conditions on the biodiesel yield. (a) Effect of the loading ratio of  $K^+$ ; (b) Effect of the molar ratio of methanol/oil; (c) Effect of the catalyst amount used; (d) Effect of the reaction temperature; (e) Effect of the reaction time. A typical reaction condition is 12:1 molar ratio of methanol/oil, 6.25 wt% load ratio of  $K^+$ /HT, and 60 °C for 1 h.

### 2.2.6. Effect of Ultrasound Aid

Figure 8a compares the effects of mechanical agitation with that of ultrasonic field aid on transesterification. Figure 8a demonstrates that the effect of ultrasonic aid on transesterification was significantly stronger than that of mechanical stirring under the same conditions. For the rapeseed oil-methanol- $K^+$ /HT reaction system, when the ultrasonic power density was 0.03 W/mL, the biodiesel yield can reach 99.9% after only five minutes of reaction time. The reaction efficiency was obviously improved. In order to achieve the same conversion rate, ultrasonic aid greatly reduced reaction time and production costs.

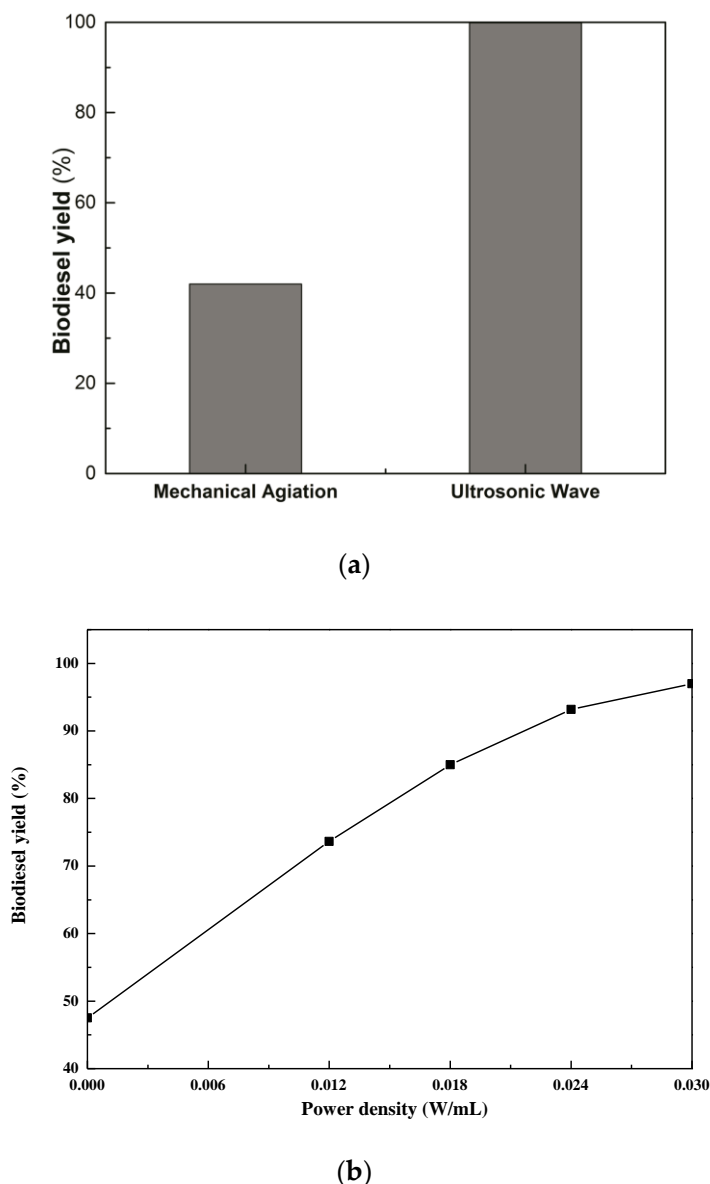


**Figure 8.** The effects of ultrasonic field aid on transesterification. (a) Mechanical agitation vs. ultrasonic field aid; (b) Effects of ultrasonic power density on biodiesel yield 12:1 molar ratio of methanol/oil, 6.25 wt% load ratio of  $K^+/HT$ , and at 60 °C for 5 min.

Ultrasound aid imparted high energy to the reaction medium through cavitation and secondary effects [31]. Physically, on the one hand, mechanical effects can promote the mixing and emulsification of oils and methanol, and increase the contact area of the two on the surface of the solid catalyst; on the other hand, cavitation bubbles collapsed and closed rapidly, accompanied by strong shock waves and micro-jets, which formed jet beams on the catalyst surface, resulting in a strong mechanical stirring effect at the phase interface [32]. This effect can break through the limitation of the laminar boundary layer, and thereby strengthen the interface renewal process and effectively maintain the activity of the catalyst. The chemical action of ultrasonic waves came from local hot spots which were generated by cavitation. The hot spot temperature can reach 5000 °C, and the spot pressure reached 50 MPa. Ultrasonic energy formed short-lived active free radicals (H and HO) from reactants or solvent molecules as the bubbles collapse [33]. That is, the polarized  $CH_3OH$  was dehydrogenated to form an active methoxy ion ( $CH_3O^-$ ), and the active  $CH_3O^-$  further attacked the first carbonyl carbon atom in

the raw material triglyceride to form a tetrahedral intermediate, thereby the progress of the reaction was further promoted.

Figure 8b shows the effects of ultrasonic power density on biodiesel yield. Readily apparent is the fact that the biodiesel yield increased with higher ultrasonic power density. As mentioned above, the cavitation of ultrasound plays an important role in the accelerating transesterification. Higher ultrasonic power density is in favour of improving the cavitation, and improves the emulsification effect of oil and methanol, resulting in smaller oil drops. Consequently, the efficiency of mass transfer and reaction rate were enhanced. However, an excessive ultrasonic density could lead to the vast vaporization of methanol, which can lower the effective concentration of methanol on the surface of catalyst. The direction of equilibrium of reaction will be reversed.

### 3. Experimental Methods

#### 3.1. Materials

Rapeseed oil with low acid value was purchased from Fujian Hua Ren oil Co., Ltd (Quanzhou, China). All the reagents, including methanol,  $\text{Mg}(\text{NO}_3)_2 \cdot 6\text{H}_2\text{O}$ ,  $\text{Al}(\text{NO}_3)_3 \cdot 9\text{H}_2\text{O}$ , NaOH, and  $\text{Na}_2\text{CO}_3$  were of analytical grade and used without further purification. They were supplied by Xilong Chemical Co., Ltd (Foshan, China).

#### 3.2. Catalysts Preparation

MgAl-HT catalysts were prepared by co-precipitation method. In a typical procedure, 0.06 mol  $\text{Mg}(\text{NO}_3)_2 \cdot 6\text{H}_2\text{O}$  and 0.03 mol  $\text{Al}(\text{NO}_3)_3 \cdot 9\text{H}_2\text{O}$  were dissolved in 100 mL distilled water which was called solution A, and 0.18 mol NaOH and 0.06 mol  $\text{Na}_2\text{CO}_3$  were dissolved in 100 mL distilled water which was called solution B. Under a vigorous yet slow stirring, solution A and B were added slowly into the three-necked flask by the constant flow pump. Then the pH of the reaction mixture was controlled. The resulting mixture was stirred vigorously at 60 °C for 24 h, then filtered and washed with water until the pH value of the filtrate close to 7. The precipitates were dried at 120 °C for twelve hours to obtain MgAl-HT. The  $\text{K}^+$ /HT catalysts were prepared by an impregnation method. MgAl-HT was mixed with a certain concentration of  $\text{K}_2\text{CO}_3$  aqueous solution and stirred for one hour, and then immersed at room temperature for 24 h. The precipitates were dried at 70 °C and calcined at 700 °C for six hours. The catalysts were labeled as  $\text{K}^+$ /HT- $x$ , where  $x$  represents the mass percentage of  $\text{K}^+$  in the catalyst ( $x = 2.50, 3.75, 5.00, 6.25, 7.50$  wt%).

#### 3.3. Catalysts Characterization

X-ray diffractograms (XRD) were recorded by a Rigaku SmartLab 3 kW diffractometer (Rigaku, Tokyo, Japan) using Cu  $\text{K}\alpha$  radiation, while operating at 40 kV and 30 mA and a scan speed of 10°/min. The IR measurement was performed on a SHIMADZU FTIR-8400s infrared meter (Kyoto, Japan) with a scan range of 4000~400  $\text{cm}^{-1}$ . The sample was compressed into self-supporting membrane with KBr to perform IR measurements. Thermo gravimetric analysis (TGA) of catalyst sample was carried out in the  $\text{N}_2$  atmosphere condition, and 20–1000 °C with a heating rate of 10 °C  $\text{min}^{-1}$  using a Shimadzu DTG-60H thermogravimetric analyzer (Kyoto, Japan). The morphology of the samples was obtained by field-emission scanning electron microscope (FESEM) using a SU8000 microscope. Nitrogen adsorption and desorption isotherms were measured by an autosorb iQ type adsorber made by Quantachrome Corporation (Boynton Beach, FL, USA). All samples were degassed at 200 °C for twelve hours under reduced pressure prior to sorption measurements. The specific surface area of the catalysts was calculated with the BrunauerEmmett-Teller (BET) method from the linear part of the nitrogen adsorption isotherms. The pore size distribution was calculated according to the Barrett-Joyner-Halenda (BJH) method from the desorption curve of the isotherm. The alkalinity of the solids was evaluated by  $\text{CO}_2$  temperature programmed desorption (TPD) using FINESORB-3010F chemical apparatus (Boynton Beach, FL, USA). The catalyst sample was heated to 200 °C for one hour

of pretreatment under high purity helium atmosphere. The CO<sub>2</sub> adsorption was performed at room temperature for one hour. The TPD experiment was carried out by heating from 30 °C to 1000 °C at 10 °C min<sup>-1</sup> in nitrogen flow.

### 3.4. Transesterification Reaction

Transesterification reactions were carried out on a batch reaction device with ultrasonic assist. A certain weight of rapeseed oil was added to a flask in advance and heated to the reaction temperature, and then a certain amount of solid base catalysts and methanol, which was in proportion to the raw oil, were placed in the flask. The mixture was heated and maintained at a definite temperature with continuous stirring or ultrasonication. Afterwards, the mixture was cooled to room temperature, and the catalysts were recovered by suction filtration. The liquid product was separated by a separating funnel. The upper layer was crude biodiesel and the lower layer was crude glycerol. The unreacted methanol was removed by rotary distillation of crude biodiesel to obtain refined biodiesel. The content of methyl esters in the ester phase was determined by the GC method using Echrom GC-A90 with the help of linear calibration curves of pure methyl esters. The biodiesel yield is calculated according to Equation (1) [20].

$$\text{yield} = \frac{m_{\text{ester}}}{m_{\text{sample}}} \times 100\% \quad (1)$$

where  $m_{\text{ester}}$  is the mass of ester in the sample calculated from the calibration curve.

Ultrasonic experiments of transesterification reaction were carried out in a bath ultrasonic device (SB-5200DTD) with an affix for keeping a constant temperature. The ultrasonic frequencies of 40 kHz, the power of 0–300 Watts, and the ultrasonic power density of 0–0.03 W/mL were employed. The reaction conditions and experimental process were similar to the above description.

## 4. Conclusions

In the study, the HT modified with K<sup>+</sup> demonstrated excellent catalytic activity for transesterification between rapeseed oil and methanol to produce biodiesel. The materials demonstrated better performance as a solid base catalyst and exhibited excellent catalytic activity in the ultrasonic wave assisted conversion system. The biodiesel yield was nearly 99% when the K<sup>+</sup> loading ratio was 6.25%, methanol/oil molar ratio was 12, K<sup>+</sup>/HT catalyst amount was 2 wt%, and the reaction conditions were 60 °C for one hour. Under the same conditions, the yield of biodiesel reached 99.9% in only five minutes with the ultrasound aid, since it can promote the enhancement of mass transfer and the formation of free radical. The incorporated K<sup>+</sup> successfully entered the lattice of Mg-Al hydrotalcite. The formation of strong alkaline active species, such as K<sub>2</sub>O, Al-O-K, and Mg-O-K significantly enhanced the alkali activity of K<sup>+</sup>/HT catalyst and produced more basic sites. Therefore, the MgAl-HT catalysts with K<sup>+</sup> doped are efficient and ideal for the synthesis of environmentally friendly biodiesel.

**Author Contributions:** Formal analysis, W.-X.Z.; investigation, C.-Y.Z.; resources, Y.L. and Y.Z.; supervision, Y.-J.L.; writing—original draft, W.-L.S.; writing—review and editing, Y.-Y.H.

**Funding:** The Industry-University-Research Collaborative Innovation Project of Xiamen (Grant No. 3502Z20183024) and the National Natural Science Foundation of China (Grant Nos. 21603077, 51603077), and the APC was funded by the National Natural Science Foundation of China (Grant No. 21603077).

**Acknowledgments:** This work was financially supported by the Industry-University-Research Collaborative Innovation Project of Xiamen (Grant No. 3502Z20183024) and the National Natural Science Foundation of China (Grant Nos. 21603077, 51603077).

**Conflicts of Interest:** There are no conflicts to declare.

## References

1. Atabani, A.E.; Silitonga, A.S.; Ong, H.C.; Mahlia, T.M.I.; Masjuki, H.H.; Badruddin, I.A.; Fayaz, H. Non-edible vegetable oils: A critical evaluation of oil extraction, fatty acid compositions, biodiesel production, characteristics, engine performance and emissions production. *Renew. Sustain. Energy Rev.* **2013**, *18*, 211–245. [[CrossRef](#)]
2. Hajjari, M.; Tabatabaei, M.; Aghbashlo, M.; Ghanavati, H. A review on the prospects of sustainable biodiesel production: A global scenario with an emphasis on waste-oil biodiesel utilization. *Renew. Sustain. Energy Rev.* **2017**, *72*, 445–464. [[CrossRef](#)]
3. Lee, A.F.; Bennett, J.A.; Manayil, J.C.; Wilson, K. Heterogeneous catalysis for sustainable biodiesel production via esterification and transesterification. *Chem. Soc. Rev.* **2014**, *43*, 7887–7916. [[CrossRef](#)] [[PubMed](#)]
4. Rawat, I.; Kumar, R.R.; Mutanda, T.; Bux, F. Biodiesel from microalgae: a critical evaluation from laboratory to large scale production. *Appl. Energy* **2013**, *103*, 444–467. [[CrossRef](#)]
5. Almeida, E.L.; Andrade, C.M.G.; dos Santos, O.A. Production of biodiesel via catalytic processes: A brief review. *Int. J. Chem. React. Eng.* **2018**, *16*, 13. [[CrossRef](#)]
6. Avhad, M.R.; Marchetti, J.M. A review on recent advancement in catalytic materials for biodiesel production. *Renew. Sustain. Energy Rev.* **2015**, *50*, 696–718. [[CrossRef](#)]
7. Mardhiah, H.H.; Ong, H.C.; Masjuki, H.H.; Lim, S.; Lee, H.V. A review on latest developments and future prospects of heterogeneous catalyst in biodiesel production from non-edible oils. *Renew. Sustain. Energy Rev.* **2017**, *67*, 1225–1236. [[CrossRef](#)]
8. Pourzolfaghar, H.; Abnisa, F.; Daud, W.M.A.W.; Aroua, M.K. A review of the enzymatic hydroesterification process for biodiesel production. *Renew. Sustain. Energy Rev.* **2016**, *61*, 245–257. [[CrossRef](#)]
9. Canakci, M.; Van Gerpen, J. Biodiesel production via acid catalysis. *Trans. ASAE* **1999**, *42*, 1203. [[CrossRef](#)]
10. Buasri, A.; Chaityut, N.; Loryuenyong, V.; Rodklum, C.; Chaikwan, T.; Kumphan, N. Continuous process for biodiesel production in packed bed reactor from waste frying oil using potassium hydroxide supported on *Jatropha curcas* fruit shell as solid catalyst. *Appl. Sci.* **2012**, *2*, 641–653. [[CrossRef](#)]
11. Pastore, C.; Barca, E.; Del Moro, G.; Lopez, A.; Mininni, G.; Mascolo, G. Recoverable and reusable aluminium solvated species used as a homogeneous catalyst for biodiesel production from brown grease. *Appl. Catal. A: Gen.* **2015**, *501*, 48–55. [[CrossRef](#)]
12. Evangelista, J.P.; Chellappa, T.; Coriolano, A.C.; Fernandes, V.J., Jr.; Souza, L.D.; Araujo, A.S. Synthesis of alumina impregnated with potassium iodide catalyst for biodiesel production from rice bran oil. *Fuel Process. Technol.* **2012**, *104*, 90–95. [[CrossRef](#)]
13. Badday, A.S.; Abdullah, A.Z.; Lee, K.T. Ultrasound-assisted transesterification of crude *Jatropha* oil using alumina-supported heteropolyacid catalyst. *Appl. Energy* **2013**, *105*, 380–388. [[CrossRef](#)]
14. Zhang, P.; Shi, M.; Liu, Y.; Fan, M.; Jiang, P.; Dong, Y. Sr doping magnetic CaO parcel ferrite improving catalytic activity on the synthesis of biodiesel by transesterification. *Fuel* **2016**, *186*, 787–791. [[CrossRef](#)]
15. Shibasaki-Kitakawa, N.; Tsuji, T.; Chida, K.; Kubo, M.; Yonemoto, T. Simple continuous production process of biodiesel fuel from oil with high content of free fatty acid using ion-exchange resin catalysts. *Energy Fuels* **2010**, *24*, 3634–3638. [[CrossRef](#)]
16. Dias, A.P.S.; Bernardo, J.; Felizardo, P.; Correia, M.J.N. Biodiesel production over thermal activated cerium modified Mg-Al hydrotalcites. *Energy* **2012**, *41*, 344–353. [[CrossRef](#)]
17. Conterposito, E.; Gianotti, V.; Palin, L.; Boccaleri, E.; Viterbo, D.; Milanese, M. Facile preparation methods of hydrotalcite layered materials and their structural characterization by combined techniques. *Inorg. Chim. Acta* **2018**, *470*, 36–50. [[CrossRef](#)]
18. Park, M.; Lee, C.I.; Lee, E.J.; Choy, J.H.; Kim, J.E.; Choi, J. Layered double hydroxides as potential solid base for beneficial remediation of endosulfan-contaminated soils. *J. Phys. Chem. Solids* **2004**, *65*, 513–516. [[CrossRef](#)]
19. Winter, F.; Xia, X.; Hereijgers, B.P.; Bitter, J.H.; van Dillen, A.J.; Muhler, M.; de Jong, K.P. On the nature and accessibility of the brønsted-base sites in activated hydrotalcite catalysts. *J. Phys. Chem. B* **2006**, *110*, 9211–9218. [[CrossRef](#)]
20. Hájek, M.; Tomášová, A.; Kocík, J.; Podzemná, V. Statistical evaluation of the mutual relations of properties of Mg/Fe hydrotalcites and mixed oxides as transesterification catalysts. *Appl. Clay Sci.* **2018**, *154*, 28–35. [[CrossRef](#)]

21. Benedictto, G.P.; Sotelo, R.M.; Dalla Costa, B.O.; Fetter, G.; Basaldella, E.I. Potassium-containing hydroxylated hydrotalcite as efficient catalyst for the transesterification of sunflower oil. *J. Mater. Sci.* **2018**, *53*, 12828–12836. [[CrossRef](#)]
22. Dossin, T.F.; Reyniers, M.F.; Berger, R.J.; Marin, G.B. Simulation of heterogeneously MgO-catalyzed transesterification for fine-chemical and biodiesel industrial production. *Appl. Catal. B: Environ.* **2006**, *67*, 136–158. [[CrossRef](#)]
23. Noiroj, K.; Intarapong, P.; Luengnaruemitchai, A.; Jai-In, S. A comparative study of KOH/Al<sub>2</sub>O<sub>3</sub> and KOH/NaY catalysts for biodiesel production via transesterification from palm oil. *Renew. Energy* **2009**, *34*, 1145–1150. [[CrossRef](#)]
24. Trakarnpruk, W.; Porntangjitlikit, S. Palm oil biodiesel synthesized with potassium loaded calcined hydrotalcite and effect of biodiesel blend on elastomer properties. *Renew. Energy* **2008**, *33*, 1558–1563. [[CrossRef](#)]
25. Xie, W.; Peng, H.; Chen, L. Transesterification of soybean oil catalyzed by potassium loaded on alumina as a solid-base catalyst. *Appl. Catal. A: Gen.* **2006**, *300*, 67–74. [[CrossRef](#)]
26. Lukić, I.; Krstić, J.; Jovanović, D.; Skala, D. Alumina/silica supported K<sub>2</sub>CO<sub>3</sub> as a catalyst for biodiesel synthesis from sunflower oil. *Bioresour. Technol.* **2009**, *100*, 4690–4696. [[CrossRef](#)]
27. Alonso, D.M.; Mariscal, R.; Moreno-Tost, R.; Poves, M.Z.; Granados, M.L. Potassium leaching during triglyceride transesterification using K/γ-Al<sub>2</sub>O<sub>3</sub> catalysts. *Catal. Commun.* **2007**, *8*, 2074–2080. [[CrossRef](#)]
28. Li, Y.; Qiu, F.; Yang, D.; Li, X.; Sun, P. Preparation, characterization and application of heterogeneous solid base catalyst for biodiesel production from soybean oil. *Biomass Bioenergy* **2011**, *35*, 2787–2795. [[CrossRef](#)]
29. Ferreira, O.P.; Alves, O.L.; Gouveia, D.X.; Souza Filho, A.G.; de Paiva, J.A.; Mendes Filho, J. Thermal decomposition and structural reconstruction effect on Mg–Fe-based hydrotalcite compounds. *J. Solid State Chem.* **2004**, *177*, 3058–3069. [[CrossRef](#)]
30. Xie, W.; Peng, H.; Chen, L. Calcined Mg–Al hydrotalcites as solid base catalysts for methanolysis of soybean oil. *J. Mol. Catal. A: Chem.* **2006**, *246*, 24–32. [[CrossRef](#)]
31. Bhangu, S.K.; Gupta, S.; Ashokkumar, M. Ultrasonic enhancement of lipase-catalysed transesterification for biodiesel synthesis. *Ultrason. Sonochem.* **2017**, *34*, 305–309. [[CrossRef](#)] [[PubMed](#)]
32. Ashokkumar, M. The characterization of acoustic cavitation bubbles—an overview. *Ultrason. Sonochem.* **2011**, *18*, 864–872. [[CrossRef](#)] [[PubMed](#)]
33. Lin, J.R.; Yen, T.F. An upgrading process through cavitation and surfactant. *Energy Fuels* **1993**, *7*, 111–118. [[CrossRef](#)]

